Enhancing the stability of albumin foam-based support baths using pectin for embedded bioprinting

IOP Publishing Biomed. Mater. 21 (2026) 015023 https://doi.org/10.1088/1748-605X/ae3a28

Biomedical Materials

PAPER

Enhancing the stability of albumin foam-based support baths using pectin for embedded bioprinting

M Rodger[1,2], É Poirier[1,2], E M A Wasmer[2], F Touani Kameni[2], S Lerouge[1,2,3,*] and A Ahmadi[1,2,*]

[1] Department of Mechanical Engineering, École de technologie supérieure, Montréal, QC, Canada
[2] Biomaterials and BioFabrication Laboratory (BBF), University of Montreal Hospital Research Center (CRCHUM), Montréal, QC, Canada
[3] Department of Radiology, Université de Montréal, Montréal, QC, Canada
[*] Authors to whom any correspondence should be addressed.

E-mail: sophie.lerouge@etsmtl.ca and ali.ahmadi@etsmtl.ca

Keywords: 3D bioprinting, embedded bioprinting, pectin, foam

OPEN ACCESS

RECEIVED
11 September 2025

REVISED
13 November 2025

ACCEPTED FOR PUBLICATION
19 January 2026

PUBLISHED
30 January 2026

Abstract

Embedded bioprinting enables the fabrication of complex, cell-laden structures by extruding bioinks into support baths. This technique has advanced the field of tissue engineering by expanding the range of printable bioinks and enabling the creation of intricate geometries; however, limitations such as instability and inadequate oxygen and nutrient delivery in current support materials restrict long print durations and compromise fidelity. Recently, albumin-based foams have been proposed as oxygen- and nutrient-permeable supports, but their rapid degradation restricts practical use. Here, we report the stabilization of albumin foams through the incorporation of pectin, a biocompatible polysaccharide. Three formulations—albumin-only (A8), albumin with 1% pectin (A8P1), and albumin with 2% pectin (A8P2)—were evaluated for foam stability, bubble morphology, rheology, and physicochemical properties. Pectin significantly delayed drainage and bubble coalescence while maintaining essential rheological features such as shear-thinning and recovery. These improvements enabled the embedded printing of chitosan, a low-viscosity and slow-crosslinking hydrogel, into multilayered and freeform structures with high fidelity. Cell viability assays confirmed that pectin did not compromise biocompatibility; A8P1 provided the most favorable microenvironment and outperformed conventional freeform reversible embedding of suspended hydrogels baths during extended incubation, owing to enhanced oxygen diffusion and a more physiological pH. Overall, pectin-stabilized albumin foams offer a simple, biocompatible, and self-removable support system that addresses key limitations of embedded bioprinting and broadens the range of printable bioinks.

1. Introduction

Three-dimensional (3D) bioprinting has emerged as a transformative tool in tissue engineering and regenerative medicine, enabling the fabrication of living constructs with spatially controlled architectures. By depositing bioinks in a layer-by-layer fashion according to a digital blueprint, it is possible to reproduce aspects of tissue organization and function [1, 2]. A central goal in the field is the creation of constructs that not only match the geometry of target tissues but also replicate their porous structure and viscoelastic properties, which strongly influence cell adhesion, proliferation, differentiation, and migration [3–7]. Despite rapid progress, the fabrication of highly complex and functional constructs remains limited by the printability of soft, low-viscosity, or slow-crosslinking bioinks. These materials, while often biologically relevant, collapse upon extrusion, yielding poor shape fidelity and resolution [8].

To overcome these challenges, embedded bioprinting was developed, in which bioinks are extruded into a secondary material, or support bath, that temporarily holds the printed material in place until it crosslinks [9–11]. This approach enables the use of a broader range of bioinks, including those that more closely mimic the native extracellular matrix, and facilitates the creation of freeform and

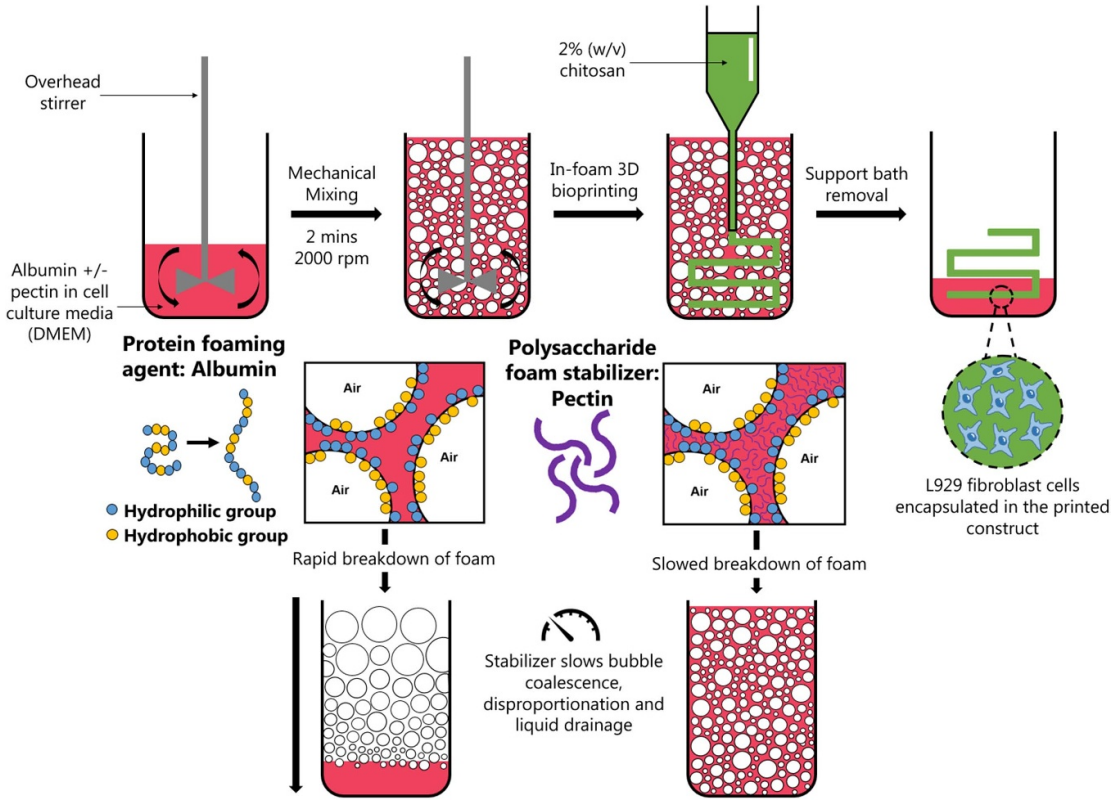

Figure 1. Schematic illustrating the in-foam bioprinting process with pectin acting as a stabilizer for the albumin-based foam.

overhanging features. Several support bath materials have been reported, such as gelatin microparticles in the freeform reversible embedding of suspended hydrogels (FRESH) technique [9], gellan gum fluid gels [12], carbopol hydrogels [13], agarose slurries [14], and pluronic blends [15, 16]. While each system has enabled important advances, common limitations remain, including insufficient oxygen and nutrient transport restricting long-term viability, and challenges with bath removal without damaging the construct [17, 18].

Recently, in-foam bioprinting has been introduced as a promising alternative, in which mechanically foamed albumin in cell culture media is used as the support bath [19]. Albumin foams offer unique biological advantages: the gas bubbles facilitate oxygen delivery, the aqueous phase maintains nutrient availability, and the inherent instability of foams allows for self-removal of the support without additional processing. Madadian *et al* demonstrated that albumin foams possess rheological properties compatible with embedded bioprinting and could sustain high cell viability. However, their practical application is limited by rapid degradation, which restricts the time window for printing more complex or large-scale constructs.

Foam stabilization has been studied extensively in the food and colloid sciences, where it is well established that protein-based foams can be reinforced by the addition of polysaccharides [20, 21]. Pectin, a high–molecular weight, anionic polysaccharide, is particularly attractive due to its biocompatibility and its ability to increase viscosity, form polymer entanglements in the continuous phase, and interact with proteins at the air–liquid interface [22, 23]. Beyond its role as a stabilizer in food foams, pectin has been widely investigated for biomedical applications such as wound healing [24], drug delivery [25], and tissue engineering [26, 27]. These properties suggest that pectin could improve foam stability without compromising the biological compatibility required for bioprinting applications.

In this study, we investigated the incorporation of pectin into albumin foams to extend their stability as embedded bioprinting support baths (figure 1). We hypothesized that pectin would reduce drainage and bubble coalescence while preserving the rheological properties essential for printing. Albumin-only foams (A8) were compared with albumin foams containing 1% or 2% pectin (A8P1, A8P2). Foam stability, bubble morphology, rheology, and physicochemical properties were characterized, and the printability of chitosan—a representative low-viscosity, slow-crosslinking hydrogel—was assessed. Finally, cell viability in printed fibroblast constructs was evaluated in comparison to traditional FRESH baths. Together, these experiments provide evidence that pectin-stabilized albumin foams represent a versatile and biologically favorable support system for embedded bioprinting.

2. Materials and methods

2.1. Foam preparation

The foam was prepared by dissolving albumin powder from chicken egg white (A5253, Sigma-Aldrich, USA) and pectin powder from citrus peel (galacturonic acid ⩾74.0%, P9135, Sigma-Aldrich, USA) in either deionized (DI) water or Dulbecco's Modified Eagle Medium (DMEM) (Gibco^{TM} DMEM/F-12, Thermo Fisher Scientific) supplemented with 10% v/v fetal bovine serum and 1% v/v antibiotics penicillin/streptomycin henceforth referred to as complete DMEM. Pectin powder was added to the solvent first and stirred at 600 rpm until completely dissolved. Albumin powder was then added, and the solution was stirred at 600 rpm for an additional 3 h to ensure complete dissolution. The solution was then mechanically mixed at 2000 rpm for 2 min using a Cole-Parmer OS-200D-C-SYS Compact Digital Mixer System (Cole-Parmer Instrument Company, Vernon Hills, IL, USA) immediately prior to all tests. Three compositions of foam were prepared for each test: 8% w/v albumin (A8), 8% w/v albumin with 1% w/v pectin (A8P1) and 8% w/v albumin with 2% w/v pectin (A8P2) (table 1).

Table 1. Compositions of the foam support baths studied.

	Albumin (% w/v)	Pectin (% w/v)
A8	8	0
A8P1	8	1
A8P2	8	2

2.2. Foam stability

To quantify the liquid drainage of the foam over time, the foam was loaded into 15 ml Falcon tubes using a syringe immediately following its preparation. The Falcon tubes were then secured inside a water bath set to 37 °C for the duration of the test. The volume of the liquid drainage accumulated at the bottom of the Falcon tube was measured at distinct time points: 0, 5, 10, 15, 20, 25, 30, 40, 50, 60, 90 and 120 min from the time the foam was prepared. For better visualization of the liquid drainage over time, as well as to see the change in bubble size over time, foams were additionally transferred into ultraviolet quartz cuvettes (Sigma-Aldrich, Oakville, ON, Canada) using a syringe immediately after their preparation and photographed at various time points.

2.3. Foam bubble size

A brightfield microscope (RVL-100-G, Echo, San Diego, CA, USA) set to 4x magnification was used to image the bubble size of the foams at various time points starting immediately after mechanically foaming: 0, 10, 30, 60, and 120 min. The foam was kept in a sealed container over the course of the experiment and a new small sample was retrieved and gently spread as a thin layer on a petri dish for imaging at each time point. This technique was used as opposed to imaging the same sample over time to ensure that the foam being imaged did not dry out, which would not properly represent the natural breakdown of foam as experienced in the in-foam bioprinting setup. For each foam composition and each time point a minimum of 3 images were taken at different locations of the sample and the diameter of a minimum of 600 bubbles were measured using ImageJ software.

2.4. Foam overrun

Foam overrun percentage was used to quantify the foamability of each foam composition (i.e. the increase in volume of the foam compared to its original liquid volume). After dissolving the powdered pectin and albumin, 15 ml of the liquid was weighed. The solution was then mechanically foamed at 2000 rpm for 2 min and 15 ml of the resulting foam was weighed. The overrun % was calculated using equation (1) as

$$\text{overrun } (\%) = 100 \times \frac{m_{\text{l}} - m_{\text{f}}}{mf}, \qquad (1)$$

where m_{l} is the mass of the liquid prior to mechanical foaming and m_{f} is the mass of the resulting foam after mechanically foaming [21].

2.5. Rheology

All rheological testing was performed on an Anton Paar rheometer (Physica MCR 301, Germany) with concentric cylinder geometry (CC10/T200). All tests were performed at 37 °C. The rheological properties of the foams were characterized using the tests outlined in the following subsections.

2.5.1. Viscosity

The viscosity of the foams (A8, A8P1, and A8P2) was measured over varying shear rates from 0.01–100 s^{-1} to confirm the foam supports exhibited shear thinning behavior. The results are plotted using a logarithmic scale.

2.5.2. Recovery

The self-recovery properties of the foam supports were characterized through cyclic recovery tests. The test was designed to mimic the cycles of deformation experienced by the foam support as the print needle passes through and returns layer-by-layer. The storage modulus (*G'*) of each foam (A8, A8P1, and A8P2) was measured through several cycles of the following: 30 s at 1% strain followed by 30 s at 100% strain followed by a sudden return to 1% strain for 30 s [15, 19]. The intervals at 1% strain mimic before and after the printing process whereas the intervals of 100% strain mimic the print needle passing through and deforming the foam.

2.6. Physiochemical characterization

2.6.1. pH

The pH of the following components of each foam composition were measured using a pH meter (LAQUAtwin, Horiba Advanced Techno, Kyoto, Japan): the liquid solution prior to mechanical foaming, the foam created from the mechanical mixing and the liquid drainage from foam as it breaks down collected from the bottom of the vessel containing the foam.

2.6.2. Osmolality

The osmolality of each foam composition was measured using an automated single-sample osmometer (3320, Advanced Instruments, Inc.). The osmometer was calibrated using a ClinitrolTM 290 reference solution (Advanced Instruments Inc., Massachusetts, USA) which has an osmolality close to physiological levels. The osmolality was measured and is reported in milliosmoles per kilogram (mOsm kg^{-1}). The liquid solution containing dissolved albumin on its own and with either 1% w/v or 2% w/v pectin before mechanical foaming were measured. Additionally, the liquid drainage resulting from the degradation of each foam composition were measured.

2.7. Chitosan hydrogel preparation

A physical thermosensitive chitosan hydrogel with gelling agent was used for both printability studies and cell studies. The chitosan was prepared following a previously published protocol [28–30]. Briefly, shrimp shell chitosan powder (ChitoClear, HQG110, Primex, Siglufjordur, Iceland) with a molecular weight of 159 kDa and degree of deacetylation of 74% was dissolved in 0.1 M hydrochloric acid (HCl) (Fisher Scientific) using an overhead stirrer for 4 h then autoclaved at 121 °C for 20 min for aseptic conditions. The gelling agent was prepared by dissolving β-glycerol phosphate (βGP, Sigma-Aldrich, USA) and sodium hydrogen carbonate (SHC, Merck KGaA, Germany) in DI water, and subsequently sterilized by filtration using a 0.22 µm pore size syringe filter (UltiDent Scientific, Canada). Both the pH of the chitosan and the gelling agent were measured using a pH meter (LAQUAtwin, Horiba Advanced Techno, Kyoto, Japan) to ensure they were in the proper ranges for use (the chitosan was only used if the pH was between 6–6.3 and between 7.4–8.4 for the gelling agent). Mixing both solutions leads to a gel precursor solution with physiological pH to which the cell suspension can be added. In the printability tests, the cell suspension was substituted with phosphate-buffered saline (PBS) 1X. Each component of the hydrogel was mixed using syringes connected by a luer lock immediately prior to printing. A volume ratio of 3:1:1 of chitosan to gelling agent to cell suspension was used, leading to a hydrogel final composition of 2% w/v Chitosan, 0.1 M βGP and 0.75 M SHC. This specific composition was selected because it leads to an *in situ* gelling hydrogel with strong mechanical properties, interconnected porosity and good cell survival and growth [28–30]. However, it is relatively slow cross-linking and has a low viscosity at room temperature prior to gelation. This means the chitosan must be physically supported once extruded through the print needle to maintain its shape for gelation.

2.8. Printability

A BioX pneumatic extrusion bioprinter (Cellink, Gothenburg, Sweden) was used with a either a $1/2''$ or $1''$ long 22G stainless steel blunt printing needle (McMaster-Carr, Elmhurst, IL, USA) with 5 mm s^{-1} printing speed and 15 kPa pressure for all printability tests. The printing pressure of 15 kPa was selected based on preliminary optimization tests, which showed that this pressure provided the most consistent and continuous extrusion of the low-viscosity chitosan bioink while avoiding over-extrusion at higher pressures and discontinuous filament formation at lower pressures. A 2% w/v chitosan hydrogel without cells, as described in section 2.7, was used for the printability study. The printhead containing the hydrogel filled cartridge was at room temperature and the print bed filled with foam was set to 37 °C permitting the chitosan to begin gelling immediately after being printed. After printing, the structures still within the foam were carefully placed in an incubator at 37 °C. Once the printed constructs were fully gelled, the foam support bath was removed using a Pasteur pipette and negative pressure. Various structures were printed to test the printability within the foam supports including, grids patterns, free-form conical structures and structures with overhanging features.

2.9. Cell studies

2.9.1. Cell culture

Mouse fibroblast L929 cells (ATCC 1 CCL-1 from Mouse Batch number 70026472) were cultured in a humidified incubator at 37 °C and 5% CO_2 using complete DMEM. Cells, passage 8–13, were subcultured into a new T75 flask upon reaching 80% confluency and detached using 0.05% trypsin/EDTA. The cell media were replaced with fresh media every 2–3 d to ensure the cells had continuous access to nutrients.

2.9.2. Chitosan bioink preparation

The 2% w/v chitosan bioinks outlined in section 2.7 consisted of a 3.33% w/v chitosan solution combined with a gelling agent solution containing 0.5 M βGP and 0.375 M SHC which was later mixed with the suspension of L929 cells. Using two syringes connected by a luer lock, the chitosan and gelling agent were mixed together with 15 back-and-forths. The resulting mixture was then mixed with the cell suspension using the same technique. A 3:1:1 (chitosan: gelling agent: cell suspension) ratio was used, resulting in a bioink with the following final concentration: 2% w/v

chitosan, 0.1 M βGP, 0.075 M SHC and either 2 or 3 M cells ml^{-1}.

2.9.3. Cell viability

The first cell study completed was to investigate if the addition of pectin had any impact on the viability of the cells encapsulated in the printed bioink. The cell laden bioink, with 3 M cells ml^{-1}, was used to extrusion print a filament into the three foam compositions (A8, A8P1 and A8P2). The printed constructs were then left for 30 min outside of the incubator, at room temperature after which the foam was removed, rinsed with PBS 1X then complete DMEM was added to the cell-laden constructs which were then placed in the humidified incubator at 37 °C and 5% CO_2. As a positive control, Control A, the bioink was printed outside of the foam, supplemented immediately with complete DMEM, and transferred directly to the incubator to demonstrate cell viability under standard culture conditions. A negative control, Control B, consisted of printing the bioink outside of the foam then waiting either 30 min or 1 h before adding cell culture media and being placed in the incubator. This control mimicked what encapsulated cells would experience during a long print taking place in open air and outside of a nutrient enriched foam bath.

A second cell study was performed to compare the cell viability when the cell-laden bioinks were printed and left in the different support baths over long periods of time. The foam supports were compared to a traditional support bath material: a gelatin microparticle slurry as used in the FRESH technique. Two versions of a FRESH support were used: one prepared using complete media as the aqueous phase (DMEM FRESH), and the other using PBS 1X (PBS FRESH). Both formulations were prepared using a previously published protocol [9] using Type A gelatin from porcine skin (MilliporeSigma, USA). Briefly, 4.5% w/v gelatin was dissolved in either complete DMEM or PBS 1X then gelled at 4 °C for 12 h. Subsequently, media or PBS was added to the gel and was blended for 2 min at pulse speed using a consumer-grade blender (Hamilton-Beach). The blended solution was then centrifuged, after which the supernatant was removed and replaced with fresh media or PBS then vortexed back into suspension. These steps were repeated until there were no more bubbles at the top of the solution after centrifugation. The chitosan bioink loaded with 2 M cells ml^{-1}, was extrusion bioprinted to create a filament into each of the 5 supports being tested: A8, A8P1, A8P2, DMEM FRESH and PBS FRESH. The printed constructs were left in the support for either 3 or 5 h at room temperature after which the supports were removed, rinsed with PBS 1X then complete DMEM was added. The prints were then placed in the humidified incubator at 37 °C and 5% CO_2.

A live/dead cell viability assay was used 24 h after the printing process to examine the viability of L929 cells embedded in the printed chitosan hydrogel for both cell studies. 2 µM of Calcein, AM (Invitrogen, Life Technologies, Carlsbad, CA, USA) and 5.5 µM of Ethidium Homodimer-1 (EthD-1, Invitrogen, Life Technologies, Carlsbad, CA, USA) in serum free DMEM were used to stain the live and dead cells respectively. The cell-laden models were incubated with the stains for 45 min before removing the stain, rinsing with PBS 1X, and then submerging in serum-free DMEM for imaging using a fluorescence microscope (RVL-100-G, Echo, San Diego, CA, USA). Three images were taken at random locations of each sample. ImageJ was used to analyze all fluorescent cell images. The green (live cells) and red (dead cells) channels of each image were normalized using a greyscale filter and appropriate thresholding of contrast and brightness levels allowed for measurements of the projected area of the red and green signals. The cell viability percentage was calculated using equation (2):

$$\text{cell viability } (\%) = 100 \times \frac{\text{live cells}}{\text{live cells} + \text{dead cells}}. \quad (2)$$

2.10. Dissolved oxygen levels

The levels of dissolved oxygen in the support baths were measured using a non-invasive optical oxygen meter (Fibox 4, PreSens Precision Sensing GmbH, Germany) equipped with PSt3 planar oxygen sensor spots (SP-PSt3-NAU, PreSens Precision Sensing GmbH, Germany) and a polymer optical fiber (PreSens Precision Sensing GmbH, Germany). The sensor spots were glued to glass cover slips with a silicone glue (SG2 silicone glue, transparent, PreSens Precision Sensing GmbH, Germany) and positioned on the surface where cell-laden constructs were printed in one of the following supports: A8, A8P1, or FRESH support bath prepared with DMEM. The salinity of each support bath was measured using an Oakton™ PC 2700 Benchtop Meter (Oakton Instruments, USA). Dissolved oxygen measurements were taken at various time points starting immediately after the printing as well as at after 1 h, 3 h, 5 h and 8 h.

2.11. Chitosan microstructure analysis

2.11.1. Scanning electron microscopy (SEM)

Using the same chitosan hydrogel as in the printability studies (see section 2.8), multi-layered grids were 3D bioprinted either in an A8P1 foam support or directly onto a printing surface without a foam support. The printed structures were left in the foam for 5 h before removing the foam, adding complete DMEM, then placing them in the incubator at 37 °C. The constructs printed outside of the foam were immediately incubated at 37 °C for 10 min to initiate gelation, after which complete DMEM was added. 24 h after printing, the hydrogels were freeze-dried (Harvest Right) overnight. The freeze-dried samples

were then secured on SEM imaging stubs using conductive tape and sputter-coated with a 20 nm gold layer (K550X Sputter Coater) and imaged using SEM S3600-N Hitachi (15 kV).

2.11.2. Histology

Similar grids were also prepared for histology. After incubation at 37 °C for 24 h to allow for complete gelation, the samples were gently washed with PBS 1X, fixed in 10% formalin for 5 min, and embedded in HistoGel™ (Thermo Fisher Scientific, USA). Samples were then enrobed in paraffin, sliced at 4 μm thickness and stained with hematoxylin and eosin (H&E) following standard histological protocols. The microstructures were examined on high resolution scan images using the Aperio ImageScope software (Leica Biosystems, IL, USA).

2.12. Statistical Analysis

All reported results represent mean values ± standard deviations of tests done at least in triplicate. The Shapiro–Wilk test was used to test for normality and skewness of the data, and Levene's test was used for equal variance. Statistical analysis of all data, except for bubble size, was performed using analysis of variance (ANOVA), with Tukey's HSD post hoc analysis to compare every two groups of data. For bubble size, Kruskall–Wallis was used, and Dunn's post hoc analysis was used to compare every two groups of data. For each test, p-values below 0.05 were considered statistically significant. All statistical analysis calculations were performed in RStudio.

3. Results and discussion

Each composition of foam studied (A8, A8P1, A8P2) contained 8% albumin and a mechanical foaming time of 2 min was chosen for all foams since previous studies have shown it provides the best results for embedded bioprinting applications [19]. Further, when higher concentrations of albumin were tested with pectin the solution became too thick, and foaming became difficult. With lower than 8% albumin, the foam was visibly less stable with liquid draining from the foam immediately after preparation.

3.1. Foam stability, bubble size and foamability

The effects of pectin addition on the physical stability of albumin foams are summarized in figure 2. As shown in figures 2(a) and (b), A8 (albumin-only) foams underwent rapid liquid drainage, with visible phase separation occurring within the first minute after foaming. In contrast, the onset of drainage was delayed to ∼30 min for A8P1 and to nearly 60 min for A8P2. This can also be seen with the quantitative measurements in figure 2(b), demonstrating that higher pectin concentrations significantly reduce drainage rates, extending foam lifetime.

Bubble size evolution further reflects this stabilizing effect (figures 2(c)–(e)). A8 exhibited a wide bubble size distribution immediately after foaming and rapid coalescence over 120 min, producing larger, heterogeneous bubbles. By comparison, both A8P1 and A8P2 maintained smaller and more uniform bubbles over time, with the 2% pectin formulation showing the narrowest distribution and slowest growth.

Foamability, measured by overrun percentage, decreased with increasing pectin concentration (figure 2(f)). While A8 produced the highest expansion, A8P1 and A8P2 generated progressively lower overrun values. This reduction is attributed to increased viscosity of the liquid phase with pectin addition, which restricts gas incorporation during whipping but enhances stability once bubbles are formed.

Taken together, these results demonstrate that pectin enhances albumin foam stability by slowing drainage and coalescence while narrowing bubble size distribution. The stabilization arises from physical mechanisms at multiple scales: (i) increased viscosity of the aqueous phase slows liquid drainage, (ii) protein–pectin complexes accumulate in the foam lamellae and Plateau borders, strengthening interfacial films against rupture, and (iii) electrostatic and steric repulsion from the polysaccharide chains hinder bubble coalescence. Similar synergistic effects of protein–polysaccharide complexes have been reported in food foams [20] and in model systems where pectin reduces drainage and disproportionation through viscosity and interfacial reinforcement [21].

It is important to note, however, that although the A8P2 composition was able to foam and created a stable foam, increasing the concentration of pectin beyond 2% w/v is not ideal. At elevated concentrations, the liquid phase becomes excessively viscous, making it increasingly difficult to incorporate air and disperse gas into bubbles during whipping. This results in poor foamability, as reflected in the lower overrun values observed with 2% pectin. Therefore, while pectin enhances stability, there is an optimal concentration window beyond which the trade-off between foamability and stability becomes unfavorable.

3.2. Rheology

For a material to be acceptable as a support bath in embedded bioprinting, it must possess key rheological properties, particularly shear-thinning behavior and the ability to recover its mechanical strength after repeated deformations. Figure 3 illustrates these properties for the albumin–pectin foams. Viscosity measurements (figure 3(a)) confirmed that all foam formulations were shear-thinning, a critical property for embedded bioprinting because it permits free nozzle movement during extrusion while ensuring

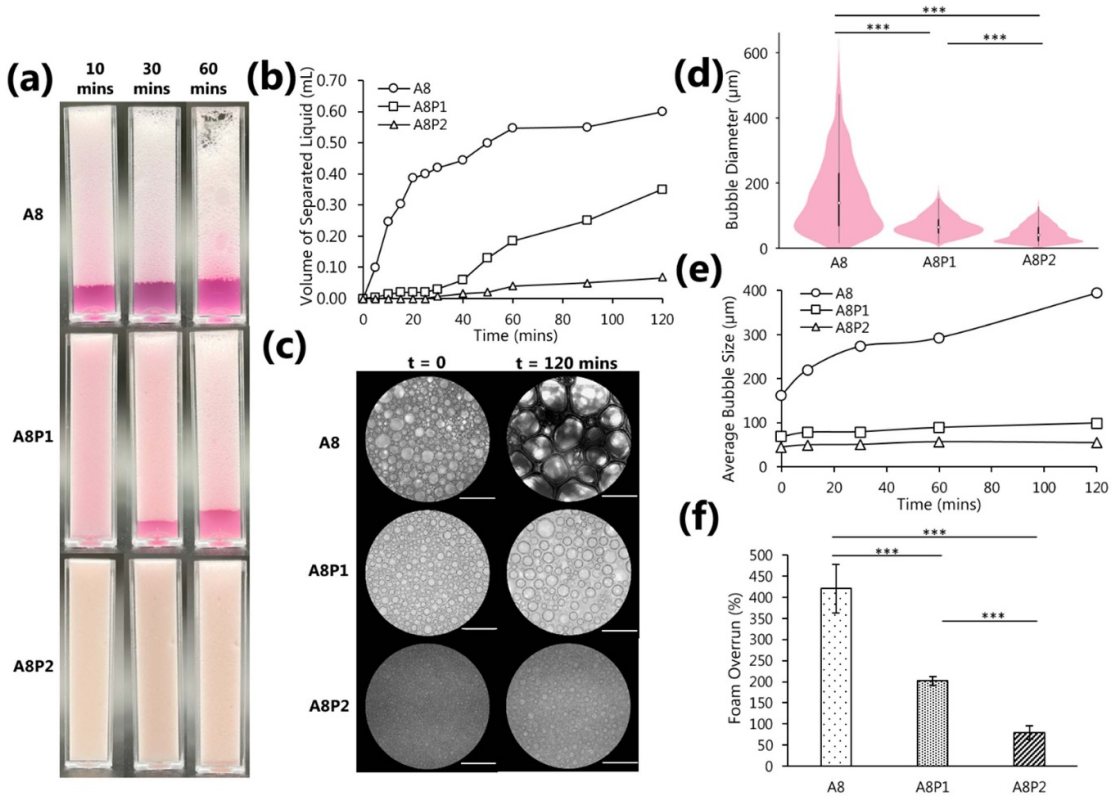

Figure 2. Physical characterization of the foam support baths. (a) Liquid drainage of foams over time (b) quantification of liquid drainage overtime from the foam in the Falcon tubes (mean values of triplicates are plotted) (c) difference in initial bubble size and bubble size after 2 h (scale bars: 1 mm) (d) initial bubble size distribution (e) average bubble size over time (f) overrun % of the foams (mean ±SD, $n = 5$, $^{*}p < 0.05$, $^{**}p < 0.01$, $^{***}p < 0.001$).

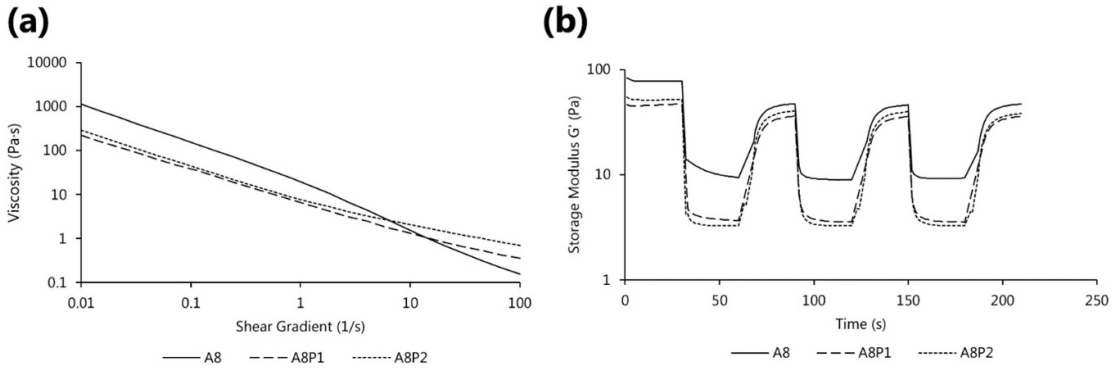

Figure 3. Rheological characterization of the foam supports. (a) Shear thinning tests: the viscosity of the foam supports as a function of shear gradient (b) recovery tests: storage moduli of the foam as a function of time through several cycles of applied strain (30 s 1% strain followed by 30 s at 100% strain repeated) (mean values of triplicates are plotted).

the bath quickly recovers its solid-like, supporting structure once the nozzle is gone [31]. The increase in low-shear viscosity with pectin addition improves the stability of the bath without compromising flowability under shear. These rheological features are consistent with previous reports on protein–polysaccharide complexes, which increase the viscoelasticity of the continuous phase and reinforce lamellae to improve foam recovery after deformation [20, 21]. The higher viscosity measured for the A8 foam can be attributed to the rapid degradation of the foam causing it to dry slightly during the measurement, increasing the measured viscosity.

In the cyclic recovery tests (figure 3(b)), all foams were able to recover their storage modulus (G') after successive cycles of strain, which simulates the passage of the print nozzle during deposition. Notably, A8P1 and A8P2 exhibited higher overall recovery of G' compared to the albumin-only foam (A8), indicating that pectin improves the resilience of the foams to repetitive deformation. This higher recovery is likely due to pectin reinforcing the bubble interfaces,

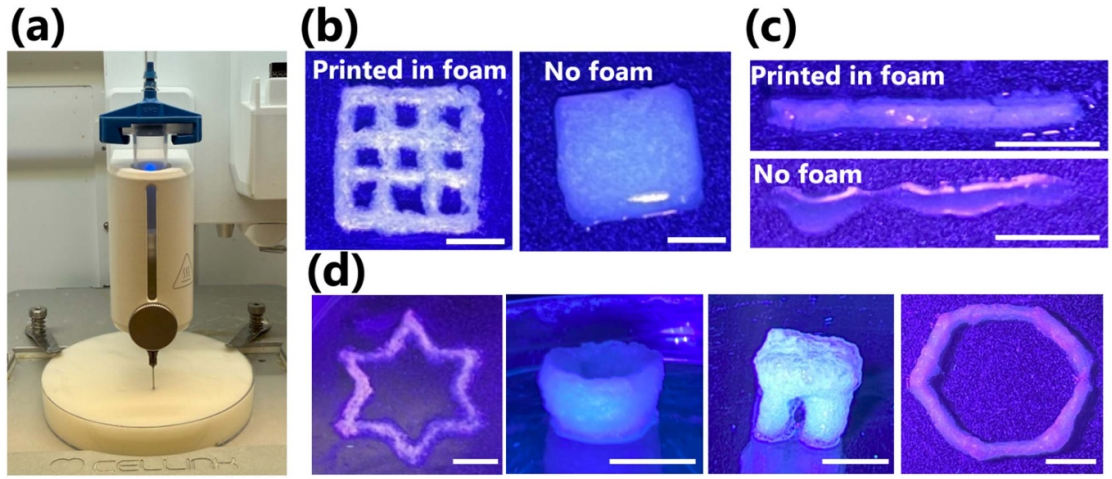

Figure 4. (a) In-foam bioprinting setup using a Cellink BIO X 3D bioprinter and 22G print needle (b) (left) chitosan grid printed in A8P1foam (right) same grid printed outside of foam support demonstrating poor printability (c) (top) filament printed in foam (bottom) filament printed outside of foam with poor printability (d) various geometries printed using chitosan into the foam supports. All scale bars are 1 cm.

allowing bubbles to stretch elastically without rupturing. In contrast, the faster liquid drainage in A8 causes it to lose structural integrity more quickly, leading to poorer recovery, consistent with earlier findings on albumin foams [19]. Compared to conventional gelatin microparticle baths used in FRESH bioprinting, the albumin–pectin foams provide a comparable rheological response but with the added advantages of oxygen diffusion and higher long-term cell viability. Thus, pectin-containing albumin foams retain the desirable rheological behavior of albumin-only foams while extending their stability and functionality for embedded bioprinting.

3.3. Printability

Chitosan, a low-viscosity and slow-crosslinking hydrogel, was printed in the albumin–pectin foams to evaluate their ability to support challenging bioinks (figure 4). The pectin-stabilized foams successfully supported multilayered and freeform structures, including filaments with overhanging features. By contrast, the same chitosan hydrogel printed outside of a support bath exhibited poor print fidelity, with even simple filaments collapsing immediately. This highlights the critical role of the support bath in enabling the use of hydrogels like chitosan, which, despite their poor standalone printability, are attractive for tissue engineering due to their biocompatibility, biodegradability [32], antimicrobial activity [33, 34], and tunability [35].

Chitosan is a polycationic polymer that is positively charged in acidic to near-neutral conditions [36]. Given that albumin carries a net negative charge in the pH range of the foams (pH levels well above 4.7 which is the isoelectric point of albumin [37]) used here, a thin residue was observed on the surface of constructs after bath removal. Because this residue interferes with quantitative shape analyses, print fidelity was assessed qualitatively rather than using a printability number ($\mathrm{Pr} = L^2/16A$ [38]). Visual inspection indicated that the constructs printed in pectin-containing foams were of comparable quality to those reported in albumin-only foam supports [19] and were consistent with other embedded bioprinting methods using granular or gel-based baths [15].

3.4. Cell viability

The first cell viability study examined whether the addition of pectin in the foam influenced the viability of chitosan-encapsulated L929 fibroblasts. As shown in figure 5, constructs printed in pectin-containing foams (A8P1 and A8P2) exhibited high cell viability, with A8P1 (1% pectin) achieving the highest viability among the three foam supports tested. The addition of pectin therefore did not negatively impact cell health. This result was expected, as pectin is well documented to be biocompatible and has been widely investigated in biomedical applications such as drug delivery, wound healing, and tissue engineering [23, 39]. These findings are also consistent with Madadian *et al* (2024), who reported that cell-laden constructs printed in albumin foam maintained high viability over time before replacement with media.

The experimental design included two controls for comparison (section 2.9.3). Control A represented standard culture conditions, where constructs were printed outside of the foam, immediately supplemented with media, and placed in the incubator. Control B mimicked an extended print in open air: constructs were printed outside of the foam, left without media for both 30 min and 1 h, and only then supplemented and incubated. In contrast, in-foam printed constructs were left in the albumin or

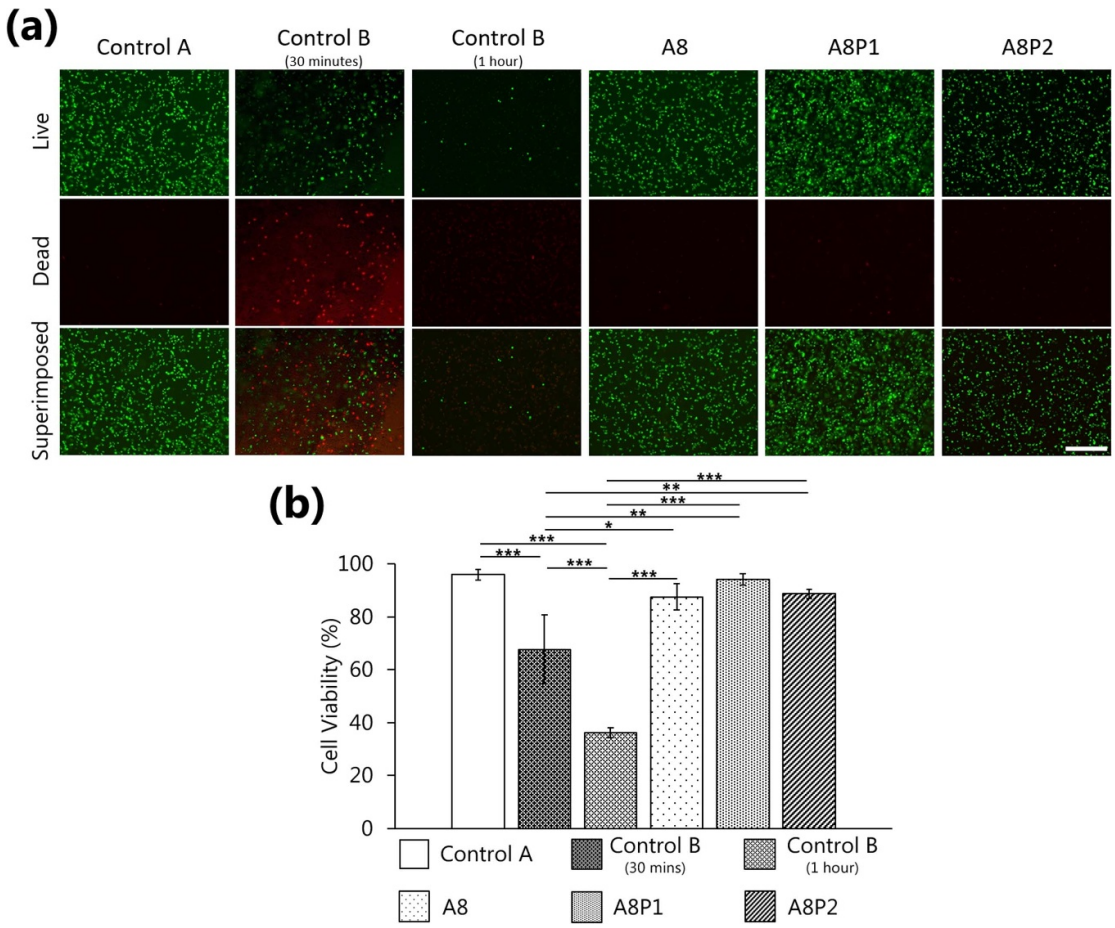

Figure 5. Impact of the addition to pectin to albumin-based foam on cell viability in chitosan bioinks. (a) Live/dead fluorescence microscopy images and (b) quantified cell viability results 24 h after the printing process. Scale bar is 200 μm. (mean ± SD, $n = 3$, $^{*}p < 0.05$, $^{**}p < 0.01$, $^{***}p < 0.001$).

albumin–pectin foams for 30 min before the support was removed, media was added, and the samples were transferred to the incubator. As illustrated in figure 5, both Control Bs (left for 30 min and 1 h) showed a drastic reduction in cell viability due to nutrient deprivation and desiccation, whereas constructs printed in the foams retained high viability. This highlights a critical advantage of in-foam embedded bioprinting: the support not only stabilizes the bioink mechanically but also provides a temporary nutrient-rich microenvironment that protects cells during and immediately after the printing process.

In the second viability study (methods described in section 2.9.3), cell-laden constructs were bioprinted directly into the different support baths and left in place for either 3 or 5 h before the supports were removed and fresh media was added. The supports tested included the three foam formulations (A8, A8P1, A8P2) and two gelatin microparticle slurries prepared according to the FRESH protocol (one with DMEM and one with PBS as the aqueous phase). This setup was designed to mimic long print durations in which cells remain embedded in the support bath for extended periods prior to media exchange.

The results are presented in figure 6. After 3 h, constructs printed in all three foams maintained high cell viability, while those printed in either version of the FRESH support exhibited poor viability. At 5 h, A8 and A8P1 still supported acceptable viability, whereas A8P2 and both FRESH conditions showed a pronounced decline. This limited long-term performance of gelatin microparticle baths has also been reported elsewhere; for example, Bessler *et al* observed a drop in HEK293 cell viability from 81% after 1 h to 48% after 2 h in a FRESH slurry [40].

These short-term cell viability studies were designed specifically to assess whether the support bath environment itself had any immediate cytotoxic or mechanical effects on the printed constructs. Long-term cell culture studies were therefore beyond the intended scope of this work, as the influence of the support bath becomes negligible once the construct is fully removed and is cultured under standard conditions for several days. Moreover, the long-term biocompatibility of the 2% chitosan bioink

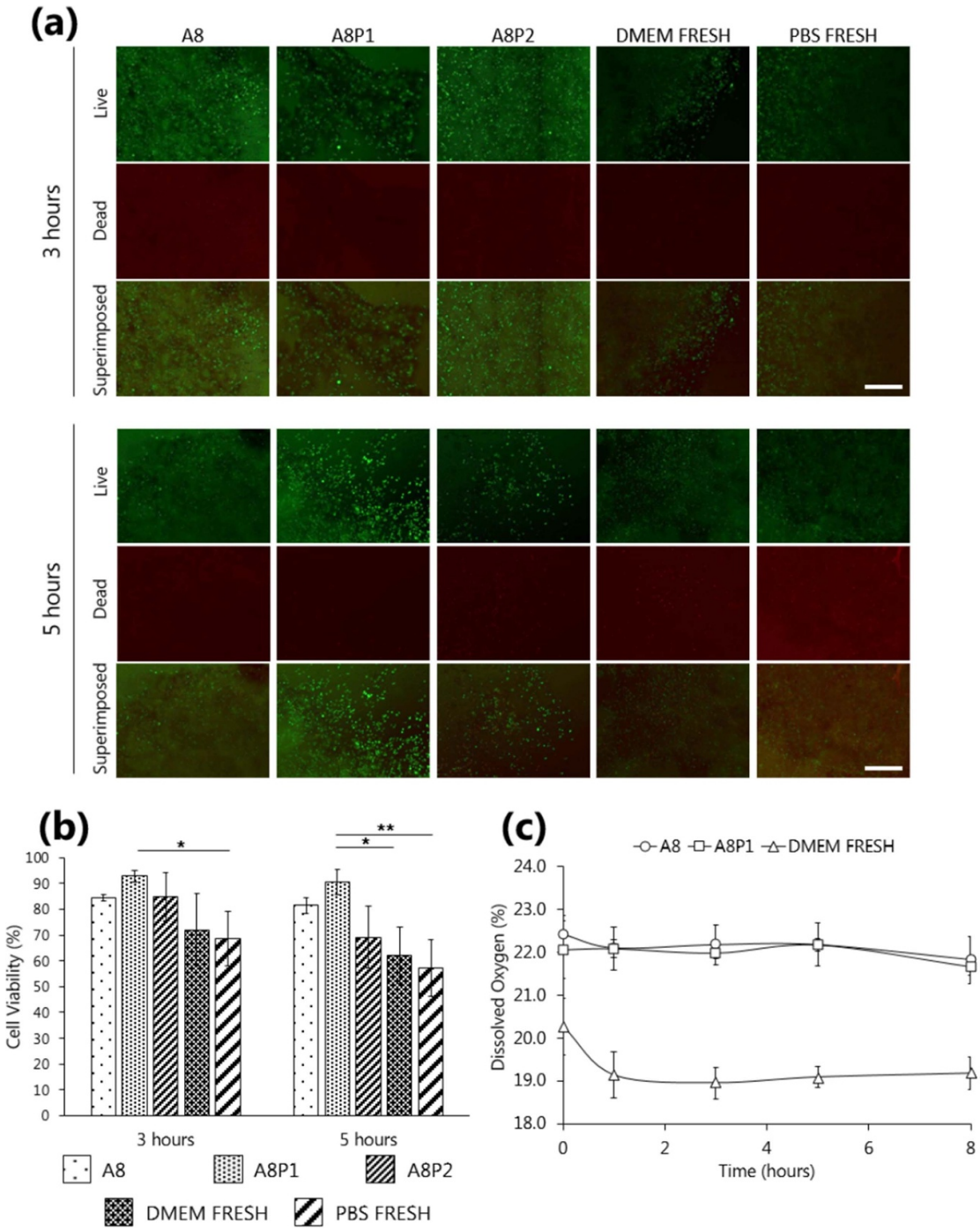

Figure 6. Comparison of foam support baths to FRESH bioprinting. L929 cells embedded into a chitosan hydrogel were printed and left in A8, A8P1, A8P2, and a FRESH support bath prepared with either DMEM or PBS 1X and left for 3 h and 5 h before replacing the support bath with cell media. (a) Fluorescent microscopy images and (b) quantification of live/dead assays completed after 24 h. (c) Dissolved oxygen content in the support baths over time with the mean value of triplicates plotted ± SD. Scale bars are 200 µm. (mean ± SD, $n = 3$, $^{*}p < 0.05$, $^{**}p < 0.01$, $^{***}p < 0.001$).

formulation used in this work has already been validated with several cell types in the past [29, 30, 41].

To further explain these findings, dissolved oxygen levels were measured in selected baths during incubation of printed constructs. A8P2 and PBS-based FRESH were excluded due to their poor viability results, leaving A8, A8P1, and DMEM-based FRESH for comparison. Foam-based supports maintained higher oxygen levels with only small decreases over time, while the FRESH bath exhibited a substantial drop (figure 6(c)). This supports the hypothesis that the porous bubble network in foams facilitates oxygen delivery, whereas the dense gelatin microparticle matrix impedes diffusion and may also hinder waste removal, leading to hypoxic conditions and reduced cell survival during extended print times. It is important to note that in this experiment, the thickness of the foam covering the printed construct

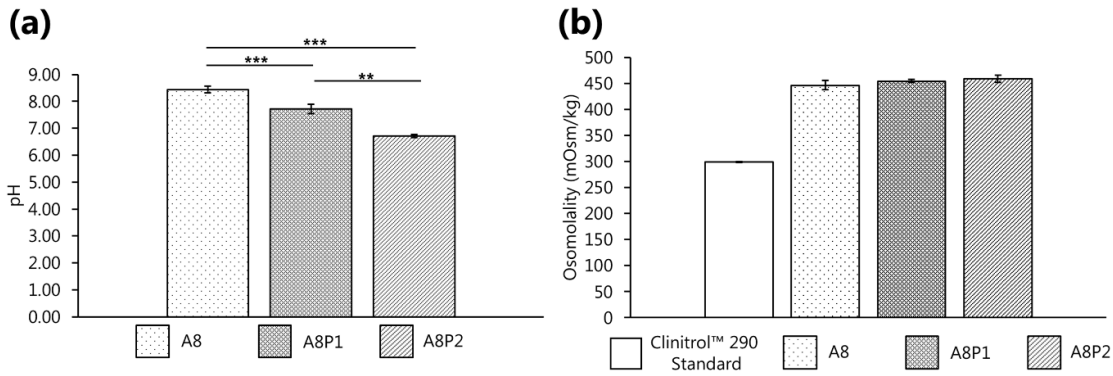

Figure 7. Physiochemical characterization of the foams (a) pH measurements of each foam composition. (mean ± SD, $n = 3$, $^{*}p < 0.05$, $^{**}p < 0.01$, $^{***}p < 0.001$) (b) Osmolality measurements of the liquid solutions for each foam composition prior to foaming in comparison to a standard solution with physiological osmolality (Clinitrol™ 290). For osmolality measurements, no significant pairwise differences were detected between the 3 foam conditions presented (Tukey HSD, all $p \geqslant 0.05$).

was relatively thin as the experiment took place in a 24 well plate. It is hypothesized that the drop in dissolved oxygen levels would be even worse given thicker coverage of the printed construct by the support bath.

3.5. Physiochemical characterization

The physiochemical properties of the foams are presented in figure 7. Increasing pectin concentration led to a progressive decrease in pH, consistent with the acidic nature of galacturonic acid residues in pectin [42]. The A8 foam had a pH of 8.44 ± 0.13, which is higher than the physiological range of 7.35–7.45 [43]. This alkalinity arises from using DMEM to prepare the foam which uses a sodium bicarbonate buffering system that requires high levels of CO_2 to maintain physiological pH. Since the foam is prepared outside an incubator, the absence of elevated CO_2 levels (5%–10% normally used in culture conditions) permits CO_2 escape, thereby increasing the pH. The stirring and high-speed mixing steps further accelerate this degassing.

In contrast, the A8P1 formulation (pH 7.71 ± 0.18) was much closer to physiological conditions and corresponded to the highest cell viability observed in section 3.6. A8P2 was slightly acidic (pH 6.72 ± 0.05), which correlated with reduced viability. This trend reflects the known sensitivity of L929 fibroblasts, which tolerate mildly alkaline conditions better than acidic ones. Indeed, Gunnink *et al* (2013) reported that increasing extracellular pH from 6 to 9 enhanced glucose uptake in these cells six-fold, suggesting greater metabolic activity under slightly basic conditions [44]. Together, these findings explain why A8P1 produced the most favorable microenvironment, followed by A8, while A8P2 was less supportive.

To confirm that pH was the main differentiating factor, the pH of the precursor solutions, foams, and drainage liquids was measured, with no statistically significant differences found between these components within each formulation. Osmolality measurements further showed no significant increase with the addition of pectin, indicating that the observed differences in cell viability are more likely attributed to pH shifts rather than osmotic stress. Overall, these results reinforce the close link between foam composition, physicochemical environment, and biological outcomes, highlighting the importance of tuning pH through stabilizer concentration for optimizing in-foam bioprinting applications.

3.6. Chitosan microstructure characterization

As shown in figure 8, the foam support bath had some influence on the microstructure of the chitosan hydrogels, especially at their surface. Constructs printed into the A8P1 foam exhibited a visibly more porous structure compared to identical chitosan hydrogels printed directly on a surface without foam. In lyophilized foam-printed samples, SEM images (figure 8(a)) revealed larger and more interconnected pores, while controls produced compact, dense microstructures with minimal internal voids. Histological analysis (figure 8(b)) also showed a rough and irregular boundary in foam-printed hydrogels, with small air-derived cavities embedded along the interface, in contrast to the smooth, continuous border observed in controls. These differences likely arise from two coupled mechanisms. First, air bubbles in the foam indent the surface of the extruded chitosan before gelation and may become transiently trapped as the hydrogel solidifies, leading to the formation of surface and internal voids. Second, electrostatic interactions between the positively charged chitosan precursor and the negatively charged albumin–pectin complexes at the foam air–liquid interface create localized adhesion points that deform the hydrogel as it gels. Protein–polysaccharide complexes such as albumin–pectin are known to adsorb strongly at bubble surfaces, increasing interfacial elasticity and modifying local microstructure; similar templating effects have been

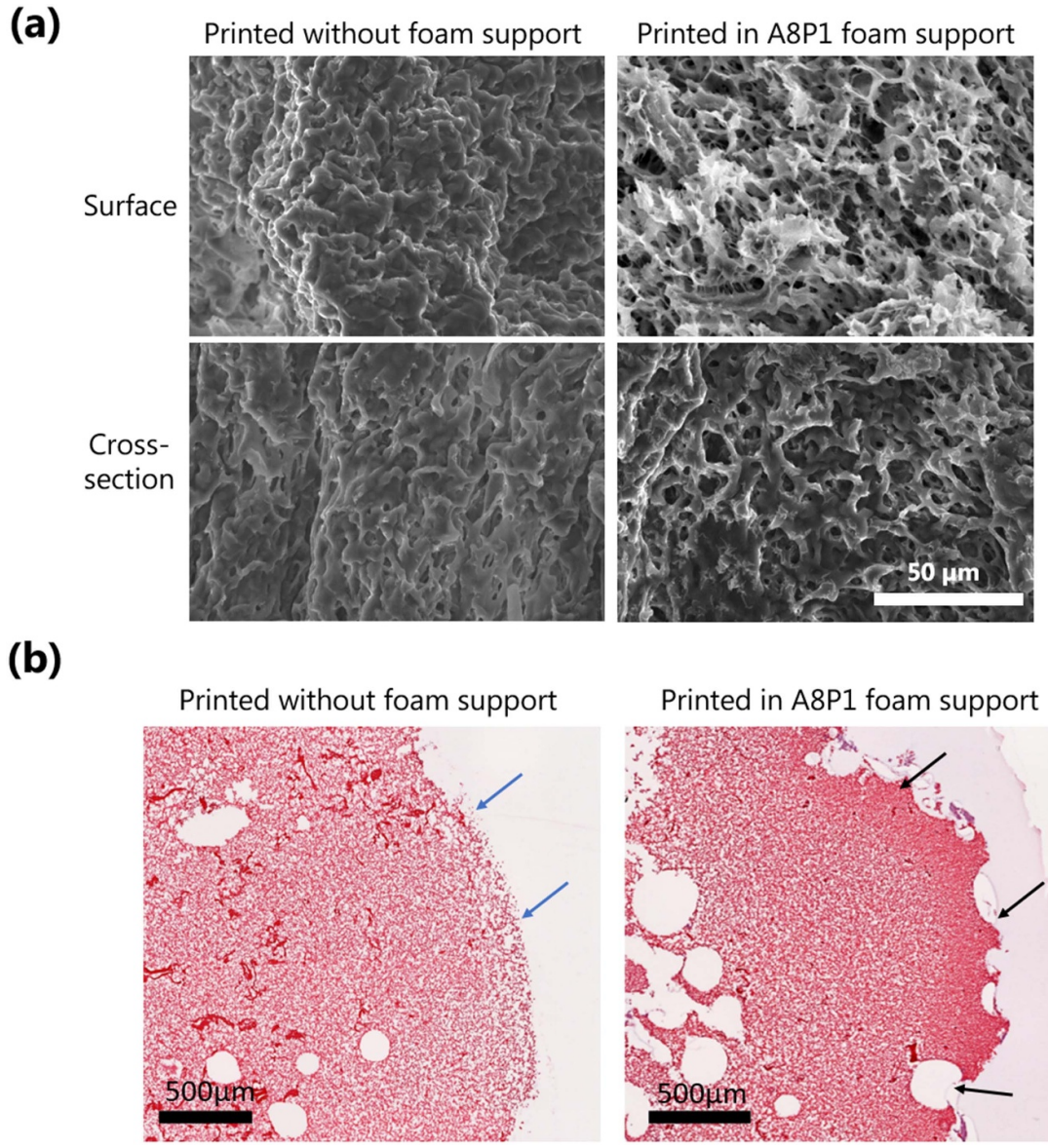

Figure 8. Microstructure characterization of the chitosan hydrogel used in the printability and cell viability studies (a) SEM imaging of the surface and cross-section of a chitosan structures printed either without a foam support (left) or inside an A8P1 foam support (right) (b) histology of chitosan hydrogel printed either with or without an A8P1 foam support.

reported in food foams and in bioprinting with granular support baths, where the microstructure of printed hydrogels correlates with the size or packing of surrounding microparticles [20, 21, 45]. These observations align with previous findings showing that support bath composition and structural features can modulate pore morphology in collagen and other bioinks [45]. The authors concluded that porosity is governed by the ratio between the shear viscosity of the ink and the zero-shear viscosity of the microgel support bath. Here, the strong viscosity of the bioink limits more or less this effect to the surface of the filament. Taken together, these results demonstrate that in-foam bioprinting not only stabilizes soft hydrogels mechanically but also serves as a microstructural templating environment, offering a simple means to modulate porosity.

Despite these promising findings, in-foam bioprinting still presents several limitations. A key practical challenge is the opacity of the foam, which makes it difficult to visually monitor the extrusion of bioink during printing. This can hinder the detection of issues such as nozzle clogging, irregular flow, or printing defects in real time. The lack of transparency also restricts the use of bioinks that require photopolymerization crosslinking, such as gelatin methacryloyl (GelMA) [46], poly(ethylene glycol) (PEG) [47], and some modified hyaluronic acid (HA)-derived hydrogels [48], since light cannot penetrate efficiently through the foam.

Looking forward, there are several avenues for optimization. The present work focused on foams prepared from chicken egg white albumin, but future efforts could investigate human-derived albumin to

improve translational potential, particularly for fabricating transplantable tissues or patient-specific disease models. Alternative foaming agents beyond albumin also remain unexplored and may broaden the range of compatible bioinks. In addition, the use of other polysaccharide stabilizers may further extend foam stability and printing windows. Together, these directions offer pathways to expand the versatility and clinical relevance of in-foam bioprinting.

4. Conclusions

This study demonstrates that incorporating pectin into albumin-based foams significantly improves their stability and performance as support baths for embedded bioprinting. The addition of pectin delayed liquid drainage, reduced bubble coalescence, and narrowed bubble size distributions, while preserving the essential rheological properties of shear-thinning behavior and rapid recovery after deformation. These physicochemical improvements enabled the successful printing of chitosan, a low-viscosity and slow-crosslinking hydrogel, into complex free-form structures with high fidelity. Importantly, the stabilized foams maintained cell viability during and after printing, outperforming conventional gelatin-based FRESH supports, particularly over extended incubation times, due to enhanced oxygen diffusion and a more favorable pH microenvironment.

Together, these results highlight albumin–pectin foams as a promising new class of support materials that combine mechanical support, nutrient permeability, and biological compatibility. By addressing longstanding challenges in embedded bioprinting, this work expands the palette of printable bioinks and opens new opportunities for fabricating functional tissue constructs. Future work should focus on translating this platform toward clinical applications by exploring human-derived albumin, alternative stabilizers, and strategies for incorporating bioinks requiring photopolymerization.

Data availability statement

The data cannot be made publicly available upon publication because they are not available in a format that is sufficiently accessible or reusable by other researchers. The data that support the findings of this study are available upon reasonable request from the authors.

Acknowledgments

This research was funded by the National Sciences and Research Council of Canada (Discovery Grant RGPIN-2023-05684 (AA) and RGPIN 2020-06684 (SL)) and Canada Foundation for Innovation (John R. Evans Leader Fund 37696). Natural Sciences and Engineering Research Council of Canada (NSERC) Canadian Graduate Scholarship—Master's (CGS M).

Author contributions

M Rodger
Conceptualization (supporting), Data curation (lead), Formal analysis (lead), Investigation (supporting), Methodology (lead), Validation (lead), Visualization (lead), Writing – original draft (lead), Writing – review & editing (lead)

É Poirier
Data curation (supporting), Investigation (supporting), Methodology (supporting), Visualization (supporting), Writing – original draft (supporting)

E M A Wasmer
Data curation (equal), Formal analysis (supporting), Methodology (supporting), Writing – review & editing (supporting)

F Touani Kameni 0000-0002-3976-2438
Data curation (equal), Formal analysis (supporting), Writing – review & editing (supporting)

S Lerouge 0000-0002-4992-5552
Conceptualization (equal), Data curation (equal), Formal analysis (supporting), Funding acquisition (supporting), Investigation (equal), Methodology (equal), Project administration (supporting), Resources (supporting), Supervision (equal), Validation (equal), Visualization (equal), Writing – original draft (equal), Writing – review & editing (equal)

A Ahmadi 0000-0003-0498-2235
Conceptualization (lead), Data curation (equal), Formal analysis (equal), Funding acquisition (lead), Investigation (lead), Methodology (equal), Project administration (lead), Resources (lead), Supervision (lead), Validation (equal), Visualization (equal), Writing – original draft (equal), Writing – review & editing (lead)

References

[1] Zeng X, Meng Z, He J, Mao M, Li X, Chen P, Fan J and Li D 2022 Embedded bioprinting for designer 3D tissue constructs with complex structural organization *Acta Biomater.* **140** 1–22
[2] Bao G, Jiang T, Ravanbakhsh H, Reyes A, Ma Z, Strong M, Wang H, Kinsella J M, Li J and Mongeau L 2020 Triggered micropore-forming bioprinting of porous viscoelastic hydrogels *Mater. Horizons* **7** 2336–47
[3] Wu D T, Jeffreys N, Diba M and Mooney D J 2022 Viscoelastic biomaterials for tissue regeneration *Tissue Eng. C* **28** 289–300

[4] Wei Q, Young J, Holle A, Li J, Bieback K, Inman G, Spatz J P and Cavalcanti-Adam E A 2020 Soft hydrogels for balancing cell proliferation and differentiation *ACS Biomater. Sci. Eng.* **6** 4687–701
[5] Chen W W et al 2017 Probing the role of integrins in keratinocyte migration using bioengineered extracellular matrix mimics *ACS Appl. Mater. Interfaces* **9** 36483–92
[6] Parmar P A, Skaalure S C, Chow L W, St-Pierre J-P, Stoichevska V, Peng Y Y, Werkmeister J A, Ramshaw J A and Stevens M M 2016 Temporally degradable collagen–mimetic hydrogels tuned to chondrogenesis of human mesenchymal stem cells *Biomaterials* **99** 56–71
[7] Courbot O and Elosegui-Artola A 2025 The role of extracellular matrix viscoelasticity in development and disease *npj Biol. Phys. Mech.* **2** 10
[8] Schwab A, Levato R, D'este M, Piluso S, Eglin D and Malda J 2020 Printability and shape fidelity of bioinks in 3D bioprinting *Chem. Rev.* **120** 11028–55
[9] Hinton T J, Jallerat Q, Palchesko R N, Park J H, Grodzicki M S, Shue H-J, Ramadan M H, Hudson A R and Feinberg A W 2015 Three-dimensional printing of complex biological structures by freeform reversible embedding of suspended hydrogels *Sci. Adv.* **1** e1500758
[10] Highley C B et al 2015 Direct 3D printing of shear-thinning hydrogels into self-healing hydrogels *Adv. Mater.* **27** 5075–9
[11] Bhattacharjee T, Zehnder S M, Rowe K G, Jain S, Nixon R M, Sawyer W G and Angelini T E 2015 Writing in the granular gel medium *Sci. Adv.* **1** e1500655
[12] Compaan A M, Song K and Huang Y 2019 Gellan fluid gel as a versatile support bath material for fluid extrusion bioprinting *ACS Appl. Mater. Interfaces* **11** 5714–26
[13] Hinton T J et al 2016 3D printing PDMS elastomer in a hydrophilic support bath via freeform reversible embedding *ACS Biomater. Sci. Eng.* **2** 1781–6
[14] Cidonio G, Cooke M, Glinka M, Dawson J, Grover L and Oreffo R 2019 Printing bone in a gel: using nanocomposite bioink to print functionalised bone scaffolds *Mater. Today Bio* **4** 100028
[15] Rahimnejad M, Adoungotchodo A, Demarquette N R and Lerouge S 2022 FRESH bioprinting of biodegradable chitosan thermosensitive hydrogels *Bioprinting* **27** e00209
[16] Hu T, Cai Z, Yin R, Zhang W, Bao C, Zhu L and Zhang H 2023 3D embedded printing of complex biological structures with supporting bath of pluronic F-127 *Polymers* **15** 3493
[17] Lee A, Hudson A, Shiwarski D, Tashman J, Hinton T, Yerneni S, Bliley J, Campbell P and Feinberg A 2019 3D bioprinting of collagen to rebuild components of the human heart *Science* **365** 482–7
[18] Shiwarski D J, Hudson A R, Tashman J W and Feinberg A W 2021 Emergence of FRESH 3D printing as a platform for advanced tissue biofabrication *APL Bioeng.* **5** 010904
[19] Madadian E, Ravanbakhsh H, Touani Kameni F, Rahimnejad M, Lerouge S and Ahmadi A 2024 In-foam bioprinting: an embedded bioprinting technique with self-removable support bath *Small Sci.* **4** 2300280
[20] Schmidt I, Novales B, Boué F and Axelos M A 2010 Foaming properties of protein/pectin electrostatic complexes and foam structure at nanoscale *J. Colloid Interface Sci.* **345** 316–24
[21] Sadahira M S, Lopes F C R, Rodrigues M I, Yamada A T, Cunha R L and Netto F M 2015 Effect of pH and interaction between egg white protein and hydroxypropymethylcellulose in bulk aqueous medium on foaming properties *Carbohydr. Polym.* **125** 26–34
[22] Miquelim J N, Lannes S C and Mezzenga R 2010 pH Influence on the stability of foams with protein–polysaccharide complexes at their interfaces *Food Hydrocol.* **24** 398–405
[23] Zhang S, Waterhouse G I, Xu F, He Z, Du Y, Lian Y, Wu P and Sun-Waterhouse D 2023 Recent advances in utilization of pectins in biomedical applications: a review focusing on molecular structure-directing health-promoting properties *Crit. Rev. Food Sci. Nutr.* **63** 3386–419
[24] Amante C, Andretto V, Rosso A, Augusti G, Marzocco S, Lollo G and Del Gaudio P 2023 Alginate-pectin microparticles loaded with nanoemulsions as nanocomposites for wound healing *Drug Deliv. Transl. Res.* **13** 1343–57
[25] Méndez D A, Schröter B, Martínez-Abad A, Fabra M J, Gurikov P and López-Rubio A 2023 Pectin-based aerogel particles for drug delivery: effect of pectin composition on aerogel structure and release properties *Carbohydr. Polym.* **306** 120604
[26] Eivazzadeh-Keihan R, Pourakbari B, Jahani Z, Aliabadi H A M, Kashtiaray A, Rahmati S, Pouri S, Ghafuri H, Maleki A and Mahdavi M 2022 Biological investigation of a novel nanocomposite based on functionalized graphene oxide nanosheets with pectin, silk fibroin and zinc chromite nanoparticles *J. Biotechnol.* **358** 55–63
[27] Morello G et al 2023 Chitosan and pectin hydrogels for tissue engineering and *in vitro* modeling *Gels* **9** 132
[28] Assaad E, Maire M and Lerouge S 2015 Injectable thermosensitive chitosan hydrogels with controlled gelation kinetics and enhanced mechanical resistance *Carbohydr. Polym.* **130** 87–96
[29] Ceccaldi C, Assaad E, Hui E, Buccionyte M, Adoungotchodo A and Lerouge S 2017 Optimization of injectable thermosensitive scaffolds with enhanced mechanical properties for cell therapy *Macromol. Biosci.* **17** 1600435
[30] Touani F K, Hamouda I, Noiseux N, Hoesli C, Der Sarkissian S and Lerouge S 2025 Injectable, cryopreservable mesenchymal stromal cell-loaded microbeads for pro-angiogenic therapy: *in vitro* proof-of-concept *Biomed. Mater.* **20** 015041
[31] Budharaju H, Sundaramurthi D and Sethuraman S 2024 Embedded 3D bioprinting–An emerging strategy to fabricate biomimetic & large vascularized tissue constructs *Bioact. Mater.* **32** 356–84
[32] Kumar A, Yadav S, Pramanik J, Sivamaruthi B S, Jayeoye T J, Prajapati B G and Chaiyasut C 2023 Chitosan-based composites: development and perspective in food preservation and biomedical applications *Polymers* **15** 3150
[33] Deng Z, Wang T, Chen X and Liu Y 2020 Applications of chitosan-based biomaterials: a focus on dependent antimicrobial properties *Mar. Life Sci. Technol.* **2** 398–413
[34] Jiménez-Gómez C P and Cecilia J A 2020 Chitosan: a natural biopolymer with a wide and varied range of applications *Molecules* **25** 3981
[35] Babu S, Shanmugavadivu A and Selvamurugan N 2024 Tunable mechanical properties of chitosan-based biocomposite scaffolds for bone tissue engineering applications: a review *Int. J. Biol. Macromol.* **272** 132820
[36] Yadav M, Kaushik B, Rao G K, Srivastava C M and Vaya D 2023 Advances and challenges in the use of chitosan and its derivatives in biomedical fields: a review *Carbohydr. Polym. Technol. Appl.* **5** 100323
[37] Guha S, Majumder K and Mine Y 2019 *Egg Proteins Encyclopedia of Food Chemistry* Melton, F Shahidi and P Varelis (Academic) pp 74–84
[38] Madadian E, Naseri E, Legault R and Ahmadi A 2024 Development of 3D-printable albumin–alginate foam for wound dressing applications *3D Print. Addit. Manuf.* **11** e1175–85
[39] Sultana N 2023 Biological properties and biomedical applications of pectin and pectin-based composites: a review *Molecules* **28** 7974
[40] Bessler N, Ogiermann D, Buchholz M-B, Santel A, Heidenreich J, Ahmmed R, Zaehres H and Brand-Saberi B 2019 Nydus One Syringe Extruder (NOSE): a Prusa i3 3D printer conversion for bioprinting applications utilizing the FRESH-method *HardwareX* **6** e00069
[41] Alinejad Y, Adoungotchodo A, Grant M P, Epure L M, Antoniou J, Mwale F and Lerouge S 2019 Injectable chitosan

hydrogels with enhanced mechanical properties for nucleus pulposus regeneration *Tissue Eng. A* **25** 303–13
[42] Mudgil D 2017 The interaction between insoluble nd soluble fiber *Dietary Fiber for the Prevention of Cdiovascular Disease* ed R A Samaan (h 3)
[43] Hopkins E, Sanvictores T and Sharma S 2018 Physiology, acid base balance
[44] Gunnink S M, Kerk S A, Kuiper B D, Alabi O D, Kuipers D P, Praamsma R C, Wrobel K E and Louters L L 2014 Alkaline pH activates the transport activity of GLUT1 in L929 fibroblast cells *Biochimie* **99** 189–94
[45] Brunel L G, Christakopoulos F, Kilian D, Cai B, Hull S M, Myung D and Heilshorn S C 2024 Embedded 3D bioprinting of collagen inks into microgel baths to control hydrogel microstructure and cell spreading *Adv. Healthcare Mater.* **13** 2303325
[46] Kumar H, Sakthivel K, Mohamed M G, Boras E, Shin S R and Kim K 2021 Designing gelatin methacryloyl (GelMA)-based bioinks for visible light stereolithographic 3D biofabrication *Macromol. Biosci.* **21** 2000317
[47] Acosta-Vélez G F, Zhu T Z, Linsley C S and Wu B M 2018 Photocurable poly (ethylene glycol) as a bioink for the inkjet 3D pharming of hydrophobic drugs *Int. J. Pharm.* **546** 145–53
[48] Ghorbani F *et al* 2023 Photo-cross-linkable hyaluronic acid bioinks for bone and cartilage tissue engineering applications *Int. Mater. Rev.* **68** 901–42